Rear interface engineering of hybrid organic-silicon nanowire solar cells via blade coating

Yi-Chun Lai,[1] Yu-Fan Chang,[1] Pei-Ting Tsai,[2] Jan-kai Chang,[3] Wei-Hsuan Tseng,[3] Yi-Cheng Lin,[1] Chu-Yen Hsiao,[1] Hsiao-Wen Zan,[1] Chih-I Wu,[3] Gou-Chung Chi,[1] and Hsin-Fei Meng,[2,4] and Peichen Yu[1,*]

[1]*Department of Photonics and Institute of Electro-Optical Engineering, National Chiao Tung University, Hsinchu 30010, Taiwan*

[2]*Institute of Physics, National Chiao-Tung University, 1001 University Rd., Hsinchu 30010 Taiwan*

[3]*Graduate Institute of Photonics and Optoelectronics, National Taiwan University, No. 1, Sec. 4, Roosevelt Rd., Taipei 10617 Taiwan*

[4]*meng@mail.nctu.edu.tw*

[*]*yup@faculty.nctu.edu.tw*

Abstract: In this work, we investigate blade-coated organic interlayers at the rear surface of hybrid organic-silicon photovoltaics based on two small molecules: Tris(8-hydroxyquinolinato) aluminium (Alq_3) and 1,3-bis(2-(4-tert-butylphenyl)-1,3,4-oxadiazol-5-yl) benzene (OXD-7). In particular, soluble Alq_3 resulting in a uniform thin film with a root-mean-square roughness < 0.2nm is demonstrated for the first time. Both devices with the Alq_3 and OXD-7 interlayers show notable enhancement in the open-circuit voltage and fill-factor, leading to a net efficiency increase by over 2% from the reference, up to 11.8% and 12.5% respectively. The capacitance-voltage characteristics confirm the role of the small-molecule interlayers resembling a thin interfacial oxide layer for the Al-Si Schottky barrier to enhance the built-in potential and facilitate charge transport. Moreover, the Alq_3 interlayer in optimized devices exhibits isolated phases with a large surface roughness, in contrast to the OXD-7 which forms a continuous uniform thin film. The distinct morphological differences between the two interlayers further suggest different enhancement mechanisms and hence offer versatile functionalities to the advent of hybrid organic-silicon photovoltaics.

OCIS codes: (160.4890) Organic materials; (310.1620) Interference coatings; (350.6050) Solar energy; (040.5350) Photovoltaic.

References and links

1. International Technology Roadmap for Photovoltaic (ITRPV) 2014 Results; 2015. Available from: http://www.itrpv.net/Reports/Downloads/2015/
2. P. V. Magazine, Photovoltaic Markets & Technology; 2012. Available from: http://www.pv-magazine.com/archive/articles/beitrag/switch-from-p-to-n-_100007072/501/#axzz3jI3NkDxM
3. Panasonic Press Release, 10 April 2014. Panasonic HIT® Solar Cell Achieves World's Highest Energy Conversion Efficiency of 25.6%. Available from: http://news.panasonic.net/stories/2014/0416_26881.html
4. M. Taguchi, A. Yano, S. Tohoda, K. Matsuyama, Y. Nakamura, T. Nishiwaki, K. Fujita, and E. Maruyama, "24.7% record efficiency HIT solar cell on thin silicon wafer," IEEE J. Photovolt. **4**(1), 96–99 (2014).
5. S. C. Shiu, J. J. Chao, S. C. Hung, C. L. Yeh, and C. F. Lin, "Morphology dependence of silicon nanowire/poly (3, 4-ethylenedioxythiophene):poly(Styrenesulfonate) heterojunction solar cells," Chem. Mater. **22**(10), 3108–3113 (2010).
6. J. C. Nolasco, R. Cabré, J. Ferré-Borrull, L. F. Marsal, M. Estrada, and J. Pallares, "Extraction of poly (3-hexylthiophene)(P3HT) properties from dark current voltage characteristics in a P3HT/n-crystalline-silicon solar cell," J. Appl. Phys. **107**(4), 044505 (2010).
7. L. He, C. Rusli, C. Jiang, H. Wang, and D. Lai, "Simple approach of fabricating high efficiency Si nanowire/conductive polymer hybrid solar cells," IEEE. Electron. Dev. Lett. **32**(10), 1406–1408 (2011).
8. X. Shen, B. Sun, D. Liu, and S. T. Lee, "Hybrid heterojunction solar cell based on organic-inorganic silicon nanowire array architecture," J. Am. Chem. Soc. **133**(48), 19408–19415 (2011).

#253576 Received 17 Nov 2015; revised 6 Jan 2016; accepted 7 Jan 2016; published 21 Jan 2016

9. T. G. Chen, B. U. Huang, E. C. Chen, P. Yu, and H. F. Meng, "Micro-textured conductive polymer/silicon heterojunction photovoltaic devices with high efficiency," Appl. Phys. Lett. **101**(3), 033301 (2012).
10. C. Xie, X. Zhang, Y. Wu, X. Zhang, X. Zhang, Y. Wang, W. Zhang, P. Gao, Y. Han, and J. Jie, "Surface passivation and band engineering: a way toward high efficiency graphene–planar Si solar cells," J. Mater. Chem. A Mater. Energy Sustain. **1**(30), 8567–8574 (2013).
11. Y. Wu, X. Zhang, J. Jie, C. Xie, X. Zhang, B. Sun, Y. Wang, and P. Gao, "Graphene Transparent Conductive Electrodes for Highly Efficient Silicon Nanostructures-Based Hybrid Heterojunction Solar Cells," J. Phys. Chem. C **117**(23), 11968–11976 (2013).
12. Y. Zhang, F. Zu, S. T. Lee, N. Zhao, and B. Sun, "Heterojunction with organic thin layers on silicon for record efficiency hybrid solar cells," Adv. Energy Mater. **4**(2), 1300923 (2014).
13. Y. Zhang, W. Cui, Y. Zhu, F. Zu, L. Liao, S. T. Lee, and B. Sun, "High efficiency hybrid PEDOT:PSS/nanostructured silicon Schottky junction solar cells by doping-free rear contact," Energy Environ. Sci. **8**(1), 297–302 (2015).
14. Y. Zhang, R. Liu, S. T. Lee, and B. Sun, "The role of a LiF layer on the performance of poly(3,4-ethylenedioxythiophene):poly(styrenesulfonate)/Si organic-inorganic hybrid solar cells," Appl. Phys. Lett. **104**(8), 083514 (2014).
15. D. Zielke, A. Pazidis, F. Werner, and J. Schmidt, "Organic-silicon heterojunction solar cells on n-type silicon wafers: the backpedot concept," Sol. Energy Mater. Sol. Cells **131**, 110–116 (2014).
16. D. Zielke, C. Niehaves, W. Lövenich, A. Elschner, M. Hörteis, and J. Schmidt, "Organic-silicon solar cells exceeding 20% efficiency," Energy Procedia **77**, 331–339 (2015).
17. Y. F. Chang, H. F. Meng, G. L. Fan, K. T. Wong, H. W. Zan, H. W. Lin, H. L. Huang, and S. F. Horng, "Blade coating of tris(8-hydroxyquinolinato)aluminum as the electron-transport layer for all-solution blue fluorescent organic light-emitting diodes," Org. Electron. **29**, 99–106 (2016).
18. J. Piao, S. Katori, T. Ikenoue, and S. Fujita, "Formation of aluminum tris(8-hydroxyquinoline) solution in methanol and fabrication of thin films by ultrasonic spray-assisted vapor deposition," Phys. Status Solidi A **209**(7), 1298–1301 (2012).
19. H. C. Card, "Aluminum—silicon Schottky barriers and ohmic contacts in integrated circuits," IEEE Trans. Electron. Dev. **23**(6), 538 (1976).
20. P. Yu, C. Y. Tsai, J. K. Chang, C. C. Lai, P. H. Chen, Y. C. Lai, P. T. Tsai, M. C. Li, H. T. Pan, Y. Y. Huang, C. I. Wu, Y. L. Chueh, S. W. Chen, C. H. Du, S. F. Horng, and H. F. Meng, "13% efficiency hybrid organic/silicon-nanowire heterojunction solar cell via interface engineering," ACS Nano **7**(12), 10780–10787 (2013).
21. J. He, P. Gao, M. Liao, X. Yang, Z. Ying, S. Zhou, J. Ye, and Y. Cui, "Realization of 13.6% efficiency on 20 μm thick Si/organic hybrid heterojunction solar cells via advanced nanotexturing and surface recombination suppression," ACS Nano **9**(6), 6522–6531 (2015).
22. M. Ikai, S. Tokito, Y. Sakamoto, T. Suzuki, and Y. Taga, "Highly efficient phosphorescence from organic light-emitting devices with an exciton-block layer," Appl. Phys. Lett. **79**(2), 156 (2001).
23. L. Hou, L. Duan, J. Qiao, W. Li, D. Zhang, and Y. Qiu, "Efficient single layer solution-processed blue-emitting electrophosphorescent devices based on a small-molecule host," Appl. Phys. Lett. **92**(26), 263301 (2008).
24. T. Yasuda, Y. Yamaguchi, D. C. Zou, and T. Tsutsui, "Carrier mobilities in organic electron transport materials determined from space charge limited current," Jpn. J. Appl. Phys. **41**(9), 5626–5629 (2002).
25. K. L. Wang, B. Lai, M. Lu, X. Zhou, L. S. Liao, X. M. Ding, X. Y. Hou, and S. T. Lee, "Electronic structure and energy level alignment of $Alq_3/Al_2O_3/Al$ and Alq_3/Al interfaces studied by ultraviolet photoemission spectroscopy," Thin Solid Films **363**(1-2), 178–181 (2000).
26. J. H. Lee, D. W. Moon, and Y. Yi, "The initial interface formation between Al and tris-(8-hydroquinoline) aluminum (Alq_3) with LiF interlayer," Org. Electron. **11**(1), 164–168 (2010).
27. Y. T. Chang, J. K. Chang, Y. T. Lee, P. S. Wang, J. L. Wu, C. C. Hsu, I. W. Wu, W. H. Tseng, T. W. Pi, C. T. Chen, and C. I. Wu, "High-efficiency small-molecule-based organic light emitting devices with solution processes and oxadiazole-based electron transport materials," ACS Appl. Mater. Interfaces **5**(21), 10614–10622 (2013).
28. X. H. Yang, F. Jaiser, S. Klinger, and D. Neher, "Blue polymer electrophosphorescent devices with different electron-transporting oxadiazoles," Appl. Phys. Lett. **88**(2), 021107 (2006).
29. L. He, L. Duan, J. Qiao, D. Zhang, L. Wang, and Y. Qiu, "Highly efficient solution-processed blue-green to red and white light-emitting diodes using cationic iridium complexes as dopants," Org. Electron. **11**(7), 1185–1191 (2010).
30. B. V. Zehbroeck, *Principles of Semiconductor Devices* (Colarado University, 2004) Chap.3.7.

1. Introduction

According to the ITRPV roadmap, n-type monocrystalline silicon photovoltaics will gradually increase its market share due to the capability for high efficiency and reliability, particularly by excluding the boron-associated photon-induced degradation in p-type Si [1,2]. Aligned with the reduced substrate thickness to save on the material cost, Panasonic Inc. has recently demonstrated a back-contact "HIT" cell with a record power conversion efficiency (PCE) of 25.6% on a 100 μm-thick n-type monocrystalline silicon wafer [3]. The term "HIT" stands for

#253576 Received 17 Nov 2015; revised 6 Jan 2016; accepted 7 Jan 2016; published 21 Jan 2016

"heterojunction with an intrinsic thin layer" of which the device structure is essentially an n-Si wafer sandwiched by wide-bandgap amorphous silicon (a-Si) materials for surface passivation and heterojunction formation. The processing temperature for HIT solar cells is less than 300 °C, which is advantageous to avoid wafer bowing and breakage issues commonly encountered for thin-silicon substrates. However, the cost of HIT solar cells is almost twice of the conventional devices due to the high-vacuum process of a-Si, which in turn limits the overall yield and throughput [4]. In this regard, solution-processed hybrid organic-silicon heterojunction photovoltaics offers an even lower process temperature (<150 °C) and more cost-effective solutions than the inorganic counterpart for the realization of high-efficiency thin-film solar cells [5–11]. Since the absorption coefficient of silicon is an order of magnitude smaller than that of the direct-bandgap semiconductors, insufficient optical absorption in thin substrates gives rise to large rear surface recombination. Therefore, one of the key aspects to achieve high PCE relies on the rear surface processing. Over the past few years, several low-temperature approaches, including rear organic interlayers and back-PEDOT heterojunction concepts have been proposed [12–16]. However, effective rear surface engineering via solution processes is still quite limited. Zhang et al. have demonstrated improved charge transport and PCE by introducing $CsCO_3$ (spin-coating), Liq (evaporation), or LiF (evaporation) between silicon and the aluminum cathode [12–14]. These approaches essentially provide an n-type doping by releasing electrons from Cs or Li ions upon their chemical reaction with Al, giving rise to a weak back surface field at the rear surface. Despite the enhanced device characteristics, $CsCO_3$ can hardly be dispersed uniformly due to its large molecules, and small-molecule Liq or LiF cannot be easily dissolved in common solvents due to poor solubility, which also limits the scalability of hybrid organic-silicon devices. In this work, we investigate other organic interlayers based on two small molecules: Tris(8-hydroxyquinolinato) aluminium (Alq_3) and 1,3-bis(2-(4-tert-butylphenyl)-1,3,4-oxadiazol-5-yl)benzene (OXD-7) via a scalable blade coating technique. In particular, a stable and soluble Alq_3 process resulting in uniform and continuous thin film (the root-mean-square, RMS roughness < 0.2nm) is demonstrated for the first time [17,18]. Either an Alq_3 or OXD-7 interlayer is next introduced into the rear surface of hybrid solar cells composed of poly(3,4-ethylenedioxythiophene): poly(styrenesulfonate) (PEDOT:PSS) spun-casted on silicon nanowire (SiNW) templates. The photovoltaic characteristics versus the blade coating speed are systematically compared, where both approaches result in a >2% net efficiency gain, representing an enhancement factor of 21.6% and 20.2% from the reference devices, respectively. The capacitance-voltage characteristics reveal the role of the small-molecule interlayers similar to a thin interfacial oxide layer for the Al-Si Schottky barrier to increase the built-in potential and facilitate the charge transport [19]. However, despite the notable characteristics improvement, the interfacial morphologies of the two materials in the best performing devices are very different. The optimized Alq_3 interlayer exhibits isolated phases with a large surface roughness, in contrast to the OXD-7, which forms a continuous uniform thin film. The distinct morphological differences between the two interlayers further suggest different enhancement mechanisms and may also be complementary to previously-reported interfacial doping materials.

2. Experimental

The general fabrication procedures of hybrid PEDOT:PSS-silicon solar cells have been described previously with slight variations on the preparation of silicon templates, organic surfactants, and metallization [7–9,20,21]. Here, we started our process by preparing silicon nanowire templates using a metal-assisted electrode-less chemical etching method [20], where n-type monocrystalline Si (100) substrates with a thickness of 650 μm and a resistivity of 5 Ω-cm were employed. Next, the templates were dipped into a dilute hydrofluoric acid (DHF, $HF:H_2O$ = 1:10) solution for 15 sec to remove the native oxide and then moved into a nitrogen-purged glove box immediately. The rear organic interlayer was to be applied through

#253576 Received 17 Nov 2015; revised 6 Jan 2016; accepted 7 Jan 2016; published 21 Jan 2016

a blade coating process. However, the small-molecule Alq_3 has been known to have very limited solubility due to its highly symmetric molecular structure; thus often requires thermal evaporation in high vacuum conditions at the cost of little material utilization [17]. In our developed process, both Alq_3 and OXD-7 powders were purchased from Lumtec Corp.. The powder was mixed with methanol as the organic solvent and then the solution was heated to 60°C for over 12 hours to completely dissolve the Alq_3 powder at the 0.1wt% and OXD-7 at the 0.2wt% concentration ratios. If a small portion of solids still precipitates, further heating to 80 °C and filtering through a Teflon filter help obtain a clear solution before the application. The silicon wafer undergone blade coating was first pre-heated at 60°C for 3 minutes to deplete the oxygen and water. Then, the blade with a groove spacing of 60 μm was mounted onto an automatically controlled stage, where the moving speed was adjusted to control the film thickness. At the beginning of the coating process, a 20 μL organic solution was first delivered from a micropipette and dropped underneath the blade, followed by blade movement at different speeds ranging from 25 to 250 mm/sec. Subsequently, hot wing was evenly blew over the surface for a quick dry off, resulting in a thin uniform film almost instantaneously. The film thickness was then measured by a microfigure measuring Instrument (ET200, Kosaka Laboratory Ltd.) with a resolution of 0.1nm in the vertical direction.

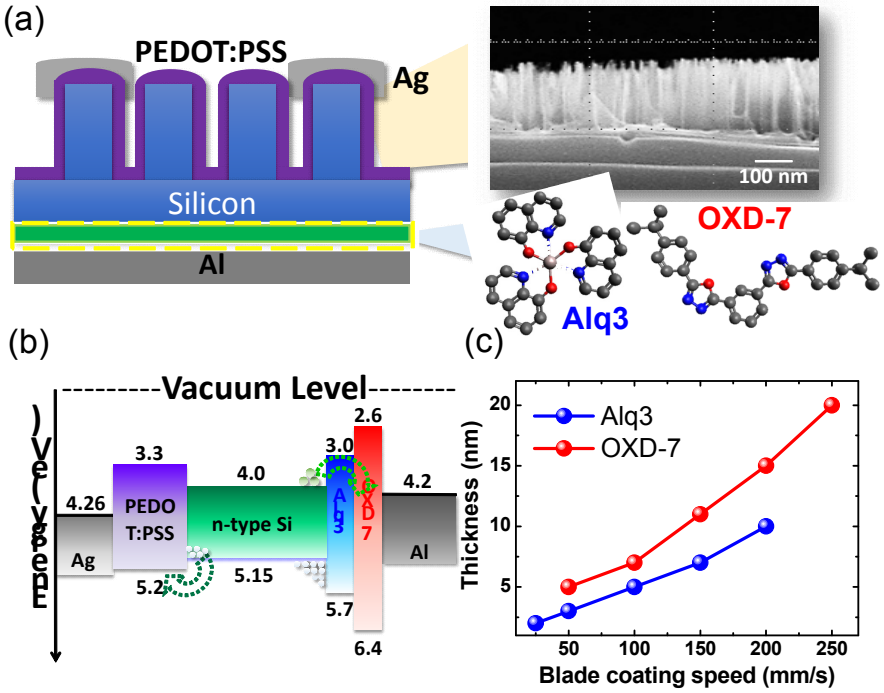

Fig. 1. (a) Schematic of a fabricated hybrid organic-silicon nanowire solar cell incorporating a rear organic interlayer. The upper inset is a cross-sectional micrograph of the conductive polymer, PEDOT:PSS laying over the silicon nanowire template, where the scale bar is 100 nm. The lower inset shows the chemical structures of the two small-molecule materials Alq_3 and OXD-7, where elements are represented by different colors: C (black), N (blue), O (red). (b) Energy band diagram of a hybrid PEDOT:PSS silicon solar cell with a Alq_3 or OXD-7 rear interlayer. (c) The thickness of the blade-coated Alq_3 and OXD-7 layer as a function of the blade coating speed.

#253576 Received 17 Nov 2015; revised 6 Jan 2016; accepted 7 Jan 2016; published 21 Jan 2016

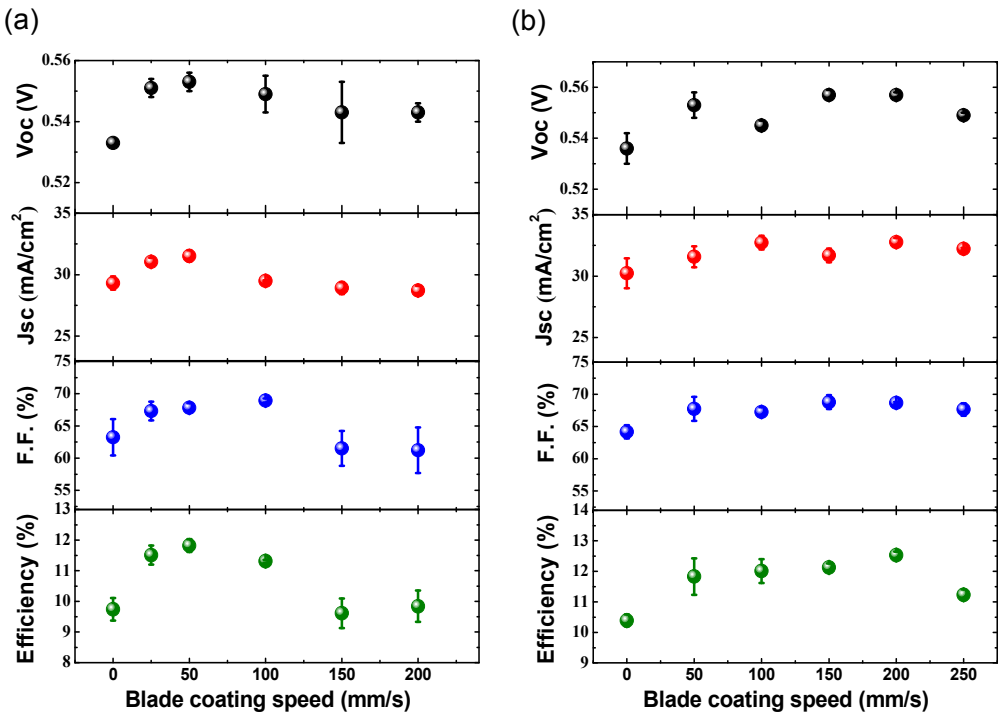

Fig. 2. Photovoltaic characteristics versus the blade coating speed, including the open-circuit voltage (V_{oc}), short-circuit current-density (J_{sc}), Fill Factor (FF), and power conversion efficiency (PCE), for the hybrid solar cells with (a) the Alq_3 and (b) the OXD-7 rear interlayers.

After the blade-coating of the small-molecule interlayer on the rear surface, a 100-nm-thick aluminum back electrode was deposited in a thermal evaporator. For the front-side process, the highly conductive aqueous PEDOS:PSS dispersion (Clevios PH1000) was prepared by mixing with 5 wt % dimethyl sulfoxide (DMSO) to enhance the conductivity and 0.3 wt % decaethylene glycol monododecyl ether (C12E10) as the surfactant. The PEDOT:PSS solution was spun-cast on top of the n-type silicon nanowire template at 8000 rpm for 100 sec, followed by hot-plate annealing at 115 °C for 10 min in ambient. Finally, 100-nm-thick silver grids as the frontal electrode were thermally evaporated through a shadow mask with a shading ratio of 18% and an opening area of 0.5 x 0.5 cm^2. Figure 1(a) shows the schematic of a fabricated device structure. The upper inset on the right shows a cross-sectional scanning electron micrograph (SEM) of nanowire arrays covered with PEDOT:PSS. On the rear side of the device, a thin layer of small-molecule materials, either Alq_3 or OXD-7, is blade-coated to the back silicon surface prior to the deposition of the aluminum cathode. The chemical structures of Alq_3 and OXD-7 are provided aside, where elements are represented by different colors: C (gray) N (blue), and O (red). Figure 1(b) shows the flat energy bands of the device layers, where OXD-7 exhibits a relatively high lowest-unoccupied-molecular-orbital (LUMO, −2.6eV) and low highest-occupied-molecular-orbital (HOMO, −6.3eV) levels, compared to those of Alq_3 (−3.0 and −5.7eV, respectively) [22,23]. Since both Alq_3 and OXD-7 have also been widely employed as the electron transport materials (ETL) for organic light emitting and photovoltaic devices, the enabling solution processes of Alq_3 and OXD-7 can facilitate the scalability and deployment of organic optoelectronic devices considerably. Figure 1(c) shows the thickness dependence of the Alq_3 and OXD-7 thin films on the coating speed. It can be seen that a faster coating speed gives

#253576 Received 17 Nov 2015; revised 6 Jan 2016; accepted 7 Jan 2016; published 21 Jan 2016

rise to a larger film thickness. Here, approximately a film thickness between 2 to 10 nm is achieved for the 0.1wt% Alq_3 and between 5 to 20nm for the 0.2wt% OXD-7 solutions.

Table 1. Best and Averaged Photovoltaic Characteristics of Hybrid Heterojunction Solar Cells with and without the Rear Alq_3 Interlayer at Different Blade Coating Speeds[a]

Alq_3 (Speed mm/sec)	V_{oc} (mV)	J_{sc} (mA/cm^2)	FF (%)	PCE (%)
REF	533.0 533.0 ± 4.1	29.5 29.3 ± 0.5	64.2 63.3 ± 2.8	10.1 9.7 ± 0.4
Alq_3 (25)	551.3 551.3 ± 3.0	31.1 31.0 ± 0.3	68.1 67.3 ± 1.5	11.7 11.5 ± 0.3
Alq_3 (50)	553.2 553.2 ± 3.2	31.6 31.5 ± 0.5	68.2 67.8 ± 0.7	11.9 11.8 ± 0.2
Alq_3 (100)	553.3 549.5 ± 6.3	29.5 29.5 ± 0.1	69.2 68.9 ± 0.3	11.3 11.3 ± 0.1
Alq_3 (150)	550.2 549.4 ± 10.1	29.2 28.9 ± 0.5	62.7 61.5 ± 2.7	10.1 9.6 ± 0.5
Alq_3 (200)	545.3 543.2 ± 3.3	28.9 28.7 ± 0.4	62.5 61.2 ± 3.5	9.9 9.8 ± 0.5

[a] The statistics are calculated by averaging four devices with a 95% confidence level.

Table 2. Best and Averaged Photovoltaic Characteristics of Hybrid Heterojunction Solar Cells with and without the Rear OXD-7 Interlayer at Different Blade Coating Speeds[a]

OXD-7 (Speed mm/sec)	V_{oc} (mV)	J_{sc} (mA/cm^2)	FF (%)	PCE (%)
REF	538.2 536.4 ± 6.1	30.4 30.2 ± 1.2	64.6 64.2 ± 1.0	10.6 10.4 ± 0.2
OXD-7 (50)	553.2 553.2 ± 5.0	31.7 31.6 ± 0.9	68.3 67.8 ± 1.8	12.0 11.8 ± 0.6
OXD-7 (100)	547.3 545.4 ± 2.3	33.0 32.7 ± 0.9	67.9 67.3 ± 0.7	12.2 12.0 ± 0.4
OXD-7 (150)	557.4 557.2 ± 2.0	32.2 31.7 ± 0.6	69.8 68.8 ± 1.1	12.5 12.1 ± 0.1
OXD-7 (200)	557.3 557.2 ± 1.4	33.0 32.8 ± 0.3	69.9 68.7 ± 1.2	12.9 12.5 ± 0.1
OXD-7 (250)	549.5 549.4 ± 1.3	32.3 32.2 ± 0.1	67.7 67.7 ± 1.0	12.1 11.2 ± 1.2

[a] The statistics are calculated by averaging four devices with a 95% confidence level.

3. Results and discussion

The statistical photovoltaic characteristics, including the short-circuit current density (J_{sc}), open-circuit voltage (V_{oc}), fill-factor (FF), and PCE, are plotted as a function of the blade coating speed for devices with the Alq_3 and with the OXD-7 interlayer as shown in Fig. 2(a) and 2(b), respectively. The reference counterpart without the rear interlayer is indicated at the zero speed. The full devices characteristics including the best and averaged values are provided Table 1 and Table 2, where the standard deviations are calculated by averaging four devices with a 95% confidence level. As shown in Fig. 2(a), the V_{oc}, J_{sc}, FF, and PCE, are all enhanced after the insertion of Alq_3 on the rear surface and peaked at the coating speed of 50 mm/sec, corresponding to an average layer thickness of 3nm in Fig. 1(c). As shown in Table 1, the averaged PCE of the hybrid solar cell with the Alq_3 interlayer is increased from the 9.7% without the interlayer, to 11.8%, mainly by boosting the averaged V_{oc} from 533.0 to 553.2 mV and the FF from 63.3% to 67.8%. As the Alq_3 layer becomes thicker, the device characteristics are quickly deteriorated. Although in Fig. 2(b) the OXD-7 devices do not show as a strong dependence on the coating speed as the Alq_3 does, the interlayer also improves the device performance considerably. The best process condition occurred at 200 mm/sec, corresponding to a thickness of ~15nm in Fig. 1(c). The averaged PCE is increased from the 10.4% without the interlayer to 12.5% with the OXD-7 where the averaged V_{oc} is improved from 536.4 to 557.2 mV and FF from 64.2% to 68.7%. In addition, the J_{sc} of the OXD-7

#253576 Received 17 Nov 2015; revised 6 Jan 2016; accepted 7 Jan 2016; published 21 Jan 2016

devices is in general larger than the referenced devices possibly due to an increased built-in potential that improves the charge carrier collection, which will be discussed later. Similar to those with the Alq3 interlayer, the devices also start to degrade when the OXD-7 thin-film becomes thicker than 15nm.

We next examine the morphology of organic thin films using atomic force microscopy (AFM) to evaluate the film quality and investigate the enhancement mechanisms behind the two small-molecule materials. Figures 3 show the topography (Figs. 3(a)-3(d)) and phase (Figs. 3(e)-3(h)) images of Alq_3 thin films resulting from a coating speed of 25, 50, 100, 200 mm/sec, respectively. The corresponding film thicknesses have been determined previously with a RMS roughness of 1.6, 2.5, 0.2, and 0.2nm. Based on the topography and phase diagrams, we indeed achieve a very continuous and uniform Alq_3 thin film using solution processes at a coating speed of 100 mm/sec, where the film thickness is as small as 5nm with a RMS roughness below 0.2nm. Such topographic specifications of the Alq_3 thin films can hardly be realized via thermal evaporation and hence is beneficial to the fabrication of organic devices at lower cost. However, by cross-referenced with the results in Fig. 2(a), the best Alq_3 devices occur at the 50 mm/sec coating speed, where the small-molecule material had yet formed a continuous network and still exhibits isolated phases. The depth differences between peaks and valleys can be as high as 25nm, suggesting that the rear aluminum electrode may still be partially in contact with the silicon, as well as the Alq_3 islands. On the other hand, Figs. 4 show the topography (Figs. 4(a)-4(d)) and phase (Figs. 4(e)-4(h)) images for the OXD-7 interlayer coated at the speeds of 50, 100, 200, and 300 mm/sec with a RMS roughness of 4.3, 0.4, 0.2, 0.2nm, respectively. The phase diagram reveals the formation of a continuous thin film at 100 mm/sec, while the best device performance occurs at 200 mm/sec.

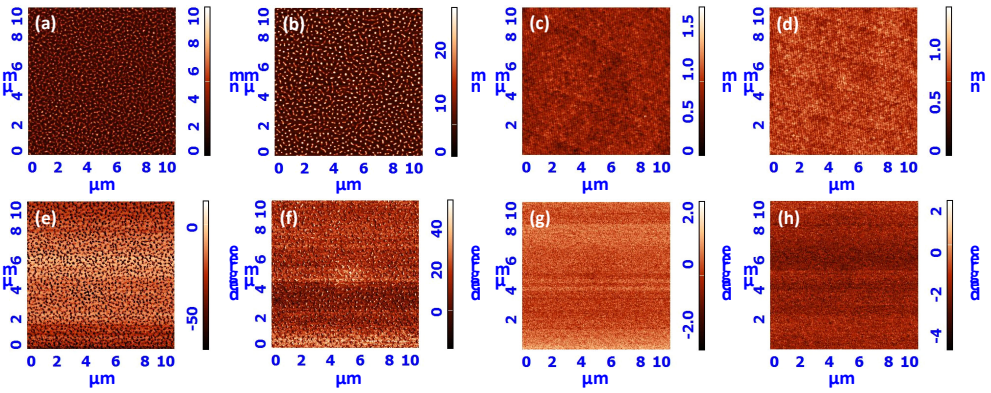

Fig. 3. (a)-(d) Topological images and (e)-(h) phase images of the Alq_3 interlayer coated on a planar silicon substrate in different blade coating speeds: 25, 50, 100, and 200 mm/s, respectively. The corresponding root mean square (RMS) roughness is 1.6, 2.5, 0.2, and 0.2 nm.

The morphological discrepancy between the optimized Alq_3 and OXD-7 interlayers suggest different mechanisms in the FF and efficiency enhancement. First, the electron mobility of OXD-7 is approximately $2.1x10^{-5}$ $cm^2/s \cdot V$, almost an order of magnitude larger than that of Alq_3 at $4.7x10^{-6}$ $cm^2/s \cdot V$ [24]. Therefore, the OXD-7 can achieve optimized transport properties with a thicker film than the Alq_3. The low electron mobility of Alq_3 also accounts for the low carrier conduction in the continuous thin film. In addition, it has been previously reported that thermally evaporated Al is diffusive into the Alq_3, which results in an interface dipole about 0.8 eV [23,24]. Giving the observation that in our devices Al may still partially contact with the Si surface and Alq_3 islands, the existence of the interfacial dipoles can locally lower the work function of the cathode without impeding charge transport. On the contrary, previous reports suggest that the chemical structure of OXD-7 has a lone pair of

#253576 Received 17 Nov 2015; revised 6 Jan 2016; accepted 7 Jan 2016; published 21 Jan 2016

oxadiazole moiety which tends to grab hot metal ions upon thermal evaporation [27]. The calculated Gibbs free energy is also negative, indicating that the chemical reaction between OXD-7 and Al is energetically favorable to generate metal complex [27]. Therefor the formation of Al-oxadiazole network is capable to facilitate interfacial charge transfer by promoting carrier extraction through the reacted oxadiazole moiety. Compared to the reference, the OXD-7 devices show a much improved FF. Finally, the large ionization potential of OXD-7 also permits the interlayer to function as a hole-blocking layer (HBL) which could increase the minority carrier lifetime and boost the V_{oc} for solar cells [28,29].

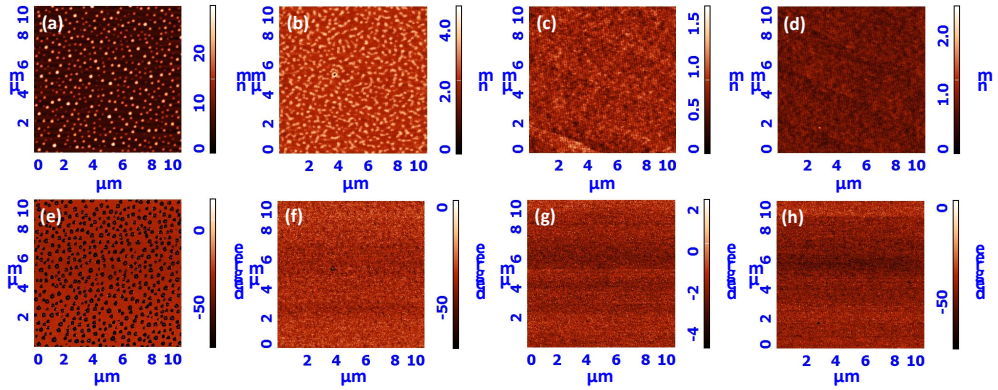

Fig. 4. (a)-(d) Topological images and (e)-(h) phase images of the OXD-7 interlayer coated on a planar silicon substrate in different blade coating speeds: 50, 100, 200, and 300 mm/s, respectively. The corresponding root mean square (RMS) roughness is 4.3, 0.4, 0.2, and 0.2 nm.

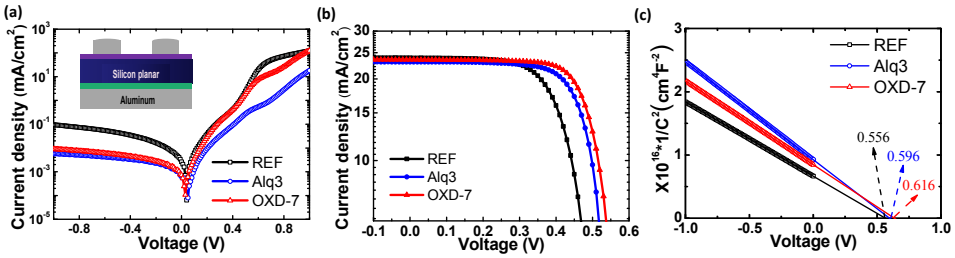

Fig. 5. (a) Dark and (b) light current density-voltage characteristics with and without the Alq_3 and OXD-7 interlayers. Inset of (a) shows a schematic of the fabricated planar device (c) Inverse square capacitance-voltage plots for planar devices with and without the Alq_3 and OXD-7 interlayers. The intersection with the x- axis yields the built-in potential across the Schottky barrier.

The characteristics of the hybrid solar cell devices with the two rear interlayers can be further explored through a capacitance-voltage (C-V) profiling technique with a modulated frequency. Upon the voltage variation, carriers are swept in and out of the depletion regions to induce a junction capacitance change. Therefore, the C-V results are informative to understand mechanisms behind the physical property changes due to modifications of materials or device structures. First of all, a simplified hybrid solar cell structure contains two depletion regions. One is located at the PEDOT:PSS/Si interface and the other at the Si/Al rear interface. The junction capacitances associated with the two depletion regions are therefore in series connection. The hybrid solar cells presented in this work employ silicon nanowire templates, which are quite complex and have a indefinable junction area at the PEDOT:PSS/Si interface. As a result, the small junction capacitance would dominate the inverse square capacitance ($1/C^2$)-voltage curve, compared to the Schottky junction

#253576 Received 17 Nov 2015; revised 6 Jan 2016; accepted 7 Jan 2016; published 21 Jan 2016

capacitance [30]. To avoid the complexity arising from the nanowire template and concentrate on the rear Al/Si Schottky barrier, we have prepared three planar devices without the rear interlayer (reference), as well as with the Alq_3 (50 mm/sec), and OXD-7 interlayers (200 mm/sec), as shown in the schematic inset of Fig. 5(a).

Table 3. Photovoltaic characteristics of planar hybrid heterojunction solar cells with and without the rear organic interlayer

Devices	V_{oc} (mV)	J_{sc} (mA/cm^2)	FF (%)	PCE (%)
REF	511.1	23.9	58.8	7.2
Alq_3	544.3	23.1	66.6	8.4
OXD-7	571.2	23.6	67.1	9.0

Figures 5(a) and 5(b) respectively plot the dark and light current density-voltage characteristics for the three planar devices. The photovoltaic characteristics under a simulated AM1.5g illumination condition is summarized in Table 3. It can be seen that the saturation current for both the Alq_3 and OXD-7 devices exhibit a ten-fold reduction, compared to the reference counterpart. Moreover, the measured V_{oc} is gained by additional 33.2 mV (Alq_3) and 60.1 mV (OXD-7) compared to the reference without the interlayer, as shown in Fig. 5(b) and Table 3. The C-V measurement from −1V to a small positive voltage is next conducted with a modulation frequency of 10kHz for the three devices, which show the characteristics of Schottky diodes [19]. The effective junction capacitance at the zero bias is about 10nF/cm^2. Figure 5(c) plots the $1/C^2$ versus the applied voltage for the three devices, which exhibits a liner dependence on the voltage at small reverse biases. The slope in a $1/C^2$-V plot for a Schottky diode is in general inversely proportional to the doping concentration of semiconductors and the intersection with the x-axis determines the built-in potential across the Schottky barrier. As shown in Fig. 5(c), the measure junction capacitance of the Alq_3 and OXD-7 devices are both smaller than the reference without significant slope changes, which indicates an additional capacitance in series with the junction capacitance [30]. The results are also different from the previous approaches with a rear back surface field, where the rear interface doping increases the junction capacitance and reduces the slope in a $1/C^2$-V plot considerably and due to the inverse doping dependence [12, 13, 26]. Therefore, our results suggest that the role of the Alq_3 or OXD-7 interlayer is analogous to a thin interfacial oxide layer for the Al/Si Schottky barrier, instead of the interfacial doping [30]. In inorganic semiconductor devices, the existence of an interfacial oxide layer reduces the Schottky barrier height and increase the built-in potential, leading to a higher current at the turn-on condition than that without the interfacial oxide [19, 30]. Here, as shown in Fig. 5(c), the built-in potential, determined by the intersection at the x-axis, is indeed increased by 40 mV (Alq_3), and 60 mV (OXD-7), respectively, which agree with the enhancement of V_{oc} shown in Fig. 5(b) very well. Finally, the incorporation of interfacial doping materials, such as LiF, Liq, and $CsCO_3$, with either Alq_3 or OXD-7 have also been investigated for organic light emitting diodes and demonstrates improvements previously [21,22]. We think that the proposed rear interfacial engineering via the solution process of Alq_3 and OXD-7 may also benefit from similar approaches.

4. Conclusion

In summary, we successfully demonstrate soluble processes for two small-molecules: Alq_3 and OXD-7 for the rear interfacial engineering of hybrid organic-silicon nanowire solar cells using a blade coating technique. The photovoltaic characteristics of the Alq_3 and OXD-7 devices exhibit enhanced open-circuit voltages and fill-factors, where the averaged power conversion efficiency achieves 11.8% and 12.5%, respectively, both corresponding to a net efficiency gain by over 2% compared to the reference devices. Through capacitance-voltage characterizations, the two rear interlayers play a role analogous to a thin interfacial oxide layer for the Al/Si Schottky barrier to increase the built-in potential and facilitate charge

#253576 Received 17 Nov 2015; revised 6 Jan 2016; accepted 7 Jan 2016; published 21 Jan 2016

transport. Moreover, the distinct morphologies between the two interlayers further suggest different enhancement mechanisms, and hence can offer versatile functionalities to the advent of hybrid organic-silicon photovoltaics.

Acknowledgments

The authors thank the Ministry of Science and Technology in Taiwan for financial support under grant number 103-2221-E-009 −166 -MY3 and 102-2221-E-009 −073 -MY3.

#253576 Received 17 Nov 2015; revised 6 Jan 2016; accepted 7 Jan 2016; published 21 Jan 2016